Online Research @ Cardiff

information services
gwasanaethau gwybodaeth

Epitaxial growth of GaSb and InAs fins on 300 mm Si (001) by Aspect Ratio Trapping

Tommaso Orzali [a], [*] Alexey Vert [b], Brendan O'Brian [b], Joshua L. Herman [c], Saikumar Vivekanand [c], Satyavolu S. Papa Rao [b] and Serge R. Oktyabrsky [c]

[a] Institute for Compound Semiconductors, Cardiff University, Queen's Buildings, The Parade Cardiff, CF24 3AA, Wales UK

[b] Suny Poly SEMATECH, 257 Fuller Rd Suite 2200, Albany, NY 12203, USA

[c] College of Nanoscale Science and Engineering, SUNY Polytechnic Institute, 251 Fuller Road, Albany, NY 12203, USA

[*] Corresponding author, email address: OrzaliT@cardiff.ac.uk

ABSTRACT:

We report on the monolithic integration of GaSb and InAs fins on on-axis 300 mm Si (001) by metal-organic chemical vapor deposition. The thickness of the GaAs/Si (001) fins used as a template is optimized to allow the formation of {111} facets and the confinement of defects generated at the GaAs/GaSb and GaAs/InAs interfaces by means of the aspect ratio trapping technique. Anti-phase domains are avoided via a careful design of the GaAs/Si interface. Threading dislocations in GaSb are controlled through the formation of an interfacial misfit dislocation array along the GaSb/GaAs $[\bar{1}11]$ and $[1\bar{1}1]$ interfaces. Defects on InAs are controlled through the promotion of a 2-dimensional growth, which spontaneously occurs on GaAs {111} planes. Results represent a step forward towards the integration of III-V nano-scale photonic and electronic components on a Si complementary metal-oxide-semiconductor compatible platform using a precisely engineered GaAs on Si template.

I. INTRODUCTION

InAs, GaSb and AlSb form a nearly lattice-matched system of III-V semiconductor materials around 6.1 Å and are often referred to as the '6.1 Å family'. The wide range of energy gaps, as well as the unique band offsets between combinations of these materials and their alloys, provide enormous flexibility in designing novel electronic and optical devices [1-3]. In particular, GaSb/InAs broken gap heterojunction Tunnel Field-Effect Transistors (TFET) with record high-ON current have recently been demonstrated [4]. Moreover, InAs and GaSb are thought to be promising candidates to replace Si in sub-7 nm Complementary Metal–Oxide–Semiconductor (CMOS) devices due to their respective high electron and hole mobilities [5-8]. In addition to low voltage operation transistors, 6.1 Å family compound semiconductors are of great interest for near- and mid-infrared optoelectronic devices [9, 10], and are considered very attractive for the fabrication of several building blocks required to develop silicon photonic platforms.

To become a realistic option for high volume manufacturing (HVM) of the next generation of CMOS and TFET devices, as well as for future applications in Si-based optoelectronic and photonic integrated circuits, III-V compound semiconductors should be integrated heterogeneously on large diameter Si (001) wafers. However, the large lattice mismatch between the 6.1 Å family and Si (~12%), together with the difference in crystal polarity and the large mismatch in thermal expansion coefficients, promote the formation of a high density of defects that affect the performance and reliability of III-V devices. One possible solution is to grow III-V epitaxial structures on their native substrates and use bonding techniques to integrate them on silicon; heterogeneous integration of GaInAsSb photodiodes coupled with silicon waveguide circuits was recently demonstrated using this approach [11]. However, wafer bonding is not the preferred strategy for the integration of high density nano-scale photonic components due to its high cost and mismatch between host substrate sizes.

Direct deposition of 6.1 Å family heterostructures on Si (001) has been demonstrated by Molecular Beam Epitaxy (MBE) using a few nm thick AlSb nucleation layer [12, 13]; misfit dislocations at the AlSb/Si interface are mainly of Lomer or 90° type, and form a regularly spaced array that efficiently relieves the mismatch stress without causing the propagation of threading dislocation (TDs) in the epitaxial layer [14-16]. Miscut substrates were used to suppress the formation of Anti-Phase Domains (APDs). Using this approach, room temperature operation of a 2.25 µm laser [17] and a 1.55 µm laser [18], both based on a GaSb

system on Si, was demonstrated under pulsed conditions. Another result worth mentioning involved the combination of both MBE and Metal-Organic Chemical Vapor Deposition (MOCVD), and used a GaP/Si (001) [19] on-axis template for the epitaxial growth of a high electron mobility AlSb/InAs heterostructure [20]. However, very few studies focused on the direct growth of GaSb on Si by MOCVD.

In a previous paper, we explored the Aspect Ratio Trapping (ART) technique to deposit high crystal quality GaAs on 300 mm Si (001) by MOCVD, achieving an excellent control of the III-V/Si interface that allowed to suppress both TDs and APDs in the heteroepitaxial layer [21]. In this study, we extend the ART technique and develop an elegant strategy to deposit 6.1 Å family compound semiconductors on Si using a GaAs/Si (001) template with optimized thickness to allow confining defects generated at the GaAs/6.1 Å family layer interface. This approach allowed us to demonstrate for the first time the monolithic integration of high crystal quality GaSb and InAs fins on 300 mm Si (001) by MOCVD and with a reduced thickness to manage the thermal mismatch. The achievement represents a step forward to enable the Very Large Scale Integration (VLSI) of high density III-V nano-scale photonic and electronic components with silicon circuits and reduce integration cost.

II.   EXPERIMENTAL DETAILS

III-V films were grown on Semiconductor Equipment and Materials International (SEMI) standard 300 mm on-axis Si (001) wafers using a showerhead MOCVD system manufactured by AIXTRON. Experimental test structures were fabricated along the [110] direction using a "short loop" process flow, which included the formation of 180 nm thermal SiO_2 on Si, followed by lithography and Reactive Ion Etching (RIE) of the oxide, to define [110] oriented trenches with an opening width of 65 nm and a pitch of 130 nm. The trench length along [110] covered the full die lithographic field dimension, or 25.4 mm.

Samples were first cleaned with a wet HF process, and subsequently subjected to a wet NH_4OH anisotropic etch, with the purpose of forming only preferential {111} Si facets at the trench bottom and obtaining a "V" shaped profile, as described in details in Ref. [21]. After the cleaning, wafers were loaded in the MOCVD tool and kept under vacuum prior to deposition. All samples were first baked at high temperature (> 800 °C) for a few minutes in pure H_2 ambient, to remove any native oxide that potentially formed during the transfer step to the MOCVD tool. The GaAs on Si template was grown at low pressure by using

trimethylgallium (TMGa) as the group-III precursors, and tertiarybutylarsine (TBAs), as well as arsine (AsH$_3$), as the group-V precursors, as described in details in Ref. [21]. The GaAs buffer thickness was optimized to allow the formation of {111} facets and ensure an aspect ratio, for the partially empty trench, high enough to trap defects that could form at the GaAs/6.1 Å family layer interface. Considering that, within the zinc-blende crystal structure, {111} stacking faults and nanotwins form an angle of ∼ 54° with the <110> directions, and that the trench width in the middle is ∼ 80 nm, we targeted a GaAs thickness of ∼ 130 nm, measured from the "V" groove bottom. This GaAs layer thickness ensured the development of {111} facets and left ∼ 120 nm inside the trench for the growth of the next layer, i.e. securing an aspect ratio of 1.5. In GaAs, {111} facets do not form immediately and intermediate steps include the coexistence of high Miller index planes that produce a rounded fin shape. Well-developed {111} facets are required to avoid trench-to-trench and run-to-run irreproduciblity of GaAs fin shapes, that would affect the growth of the 6.1 Å family heteroepitaxial layer.

GaAs (001) is a relatively usual substrate to grow high crystal quality blanket GaSb films by MBE [22-24]. Under appropriate growth conditions, the strain energy associated with the 7.8% lattice mismatch is relaxed through the formation of a periodic array of 90° Lomer misfit dislocations at the GaSb/GaAs [001] interface, which largely hinders the formation of threading dislocations. As a result, the threading dislocation density can be reduced to about (3-5) x 10^8 cm^{-2} at the surface of ∼1.5 μm thick structures [25, 26] from 3 x 10^{12} cm^{-2} (equivalent to 5.6 nm period of misfit dislocation) at the relaxed hetero-interface. The interfacial misfit (IMF) growth mode was successfully demonstrated as well by MOCVD, where a 300 nm thick GaSb layer with a low density of dislocations was achieved again on GaAs (001) [27-28]. In this study we attempt to grow for the first time GaSb on GaAs {111}-facetted surface on Si (001), with the purpose of investigating whether a similar IMF relaxation mechanism occurs at the GaSb/GaAs <111> interfaces, that would promote the growth of high quality GaSb.

The optimal growth conditions for GaSb were found to be the following: after the deposition of the GaAs buffer, the temperature was decreased to 520 °C and the AsH$_3$ flux was interrupted to remove excess arsenic from the GaAs surface by exposing it for 30 seconds to H$_2$. As discussed in Ref. [28], this is a critical step to avoid the formation of a GaAsSb intermixing layer at the interface that would lead to non-IMF growth conditions. Moreover, the V/III ratio must be carefully controlled to avoid the formation of gallium

droplets or antimony hillocks. An ideal V/III flux ratio of 1.6 was used in this development with TESb as the group-V precursor.

III. RESULTS AND DISCUSSION

Figure 1a shows the Bright Field (BF) Scanning Transmission Electron Microscope (STEM) image of the cross section of GaSb on GaAs on Si fins along $[1\bar{1}0]$, the direction perpendicular to the trenches, together with the Energy Dispersive X-Ray Spectroscopy STEM-EDS map of the Arsenic Kα and the Antimony Lα peaks. The good overall morphology and thickness uniformity denote a low density of defects reaching the GaSb surface in the sample portion investigated, with the exception of a few slightly taller fins with an irregular shape. Figure 1b shows the higher magnification bright field STEM image of the same cross section along $[1\bar{1}0]$. As described in detail in Ref. [21], a deep (~ 75 nm) "V" shaped groove forms on silicon as a consequence of the NH$_4$OH etch, with {111} facets extensively undercutting the SiO$_2$ sidewalls. The GaAs buffer layer appears brighter than GaSb in the STEM image, due to the lighter atomic weight of As compared to Sb; GaAs fins expose {111} facets and a rounded top made of higher Miller index planes, {112} and {113}. The GaAs fin height is ~ 150 nm, measured from the top to the V shaped bottom. Increasing the GaAs thickness does not help preventing fin top rounding, as demonstrated in Ref. [21], where fins were 225 nm tall. The dark shades at the GaAs/Si interface are an indication of epitaxial stress due to the misfit dislocations, as well as threading segments and stacking faults which would annihilate at the oxide sidewalls if the GaAs fins were taller. As a consequence, a few {111} defects reach the interface with GaSb, but don't propagate further due to even higher strain field. GaSb fins are flat and mainly expose the (001) surface; the formation of {111} facets is kinetically inhibited by the low deposition temperature used for GaSb, as mean surface diffusion length in the $[1\bar{1}0]$ direction limits the extent to which the facets can coarsen. A few {111} defects form at the interface with GaAs and propagate through the GaSb layer. They would ultimately annihilate at the oxide sidewalls if GaSb fins were slightly thicker than the measured 80 nm.
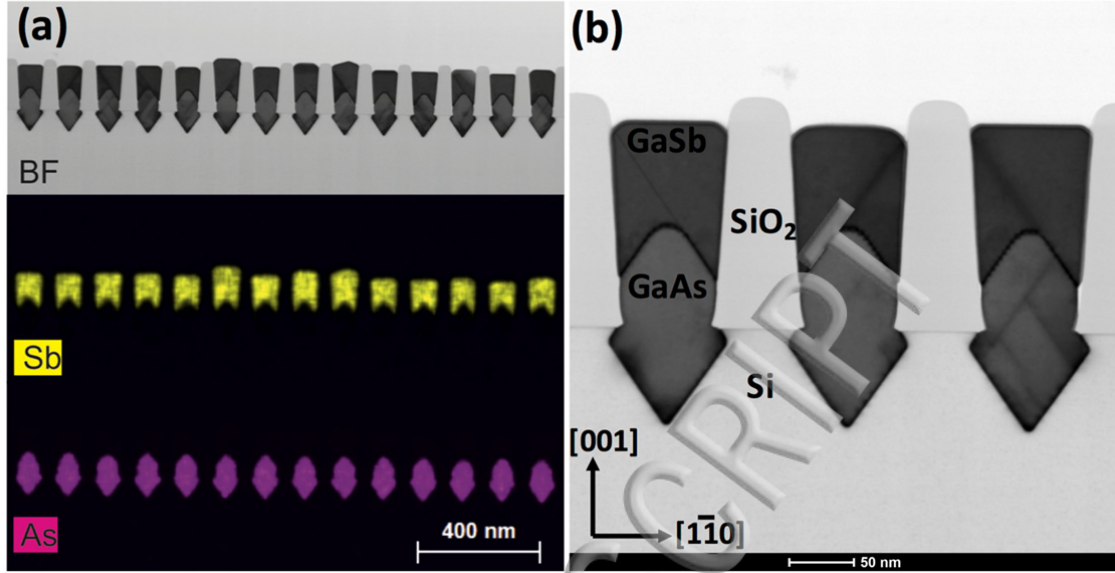
Figure 1: (a) Bright Field (BF) STEM image of the cross section of GaSb on GaAs on Si fins along $[1\bar{1}0]$, together with the Energy Dispersive X-Ray Spectroscopy STEM-EDS map of the Arsenic Kα and the Antimony Lα peaks. (b) Higher magnification Bright Field (BF) STEM image of three GaSb fins.

The higher magnification bright-field STEM image of the GaSb/GaAs interface (Fig. 2a) shows regularly spaced 60° dislocation array imaged edge-on with a period of 4.8 nm along the interface, corresponding to the match of 13 GaSb with 14 GaAs (111) lattice planes. As already mentioned, under specific growth conditions, GaSb deposited on planar GaAs (001) produces a periodic array of 90° misfit dislocations along both [110] and $[1\bar{1}0]$ directions, which are energetically favorable compared to 60° dislocations, although their formation can be affected by nucleation kinetics [29, 30]. In our case, the misfits dislocations are of mixed 60° type as evident from the plotted Burgers circuit around one of the dislocation in Fig. 2(a). The circuit is represented by a thick black line; its closure gap corresponds to the projection of Burger's vector on the plane of figure. This projection is the edge component of the Burgers vector $b_{edge} = \frac{a}{4}[\bar{1}\bar{1}2]$, which is responsible for misfit strain relaxation. To complete the Burgers vector of a perfect dislocation in face-centered cubic (FCC) structure, the screw component normal to the figure plane, $b_{screw} = \frac{a}{4}[\bar{1}10]$ or $= \frac{a}{4}[1\bar{1}0]$, should be added confirming the 60° nature of misfit dislocations with $b_1 = \frac{a}{2}[\bar{1}0\bar{1}]$ or $\frac{a}{2}[0\bar{1}\bar{1}]$ [28]. The triangle shape of the interface gives rise to the second array of 60° misfit dislocations on

6

the other face of the fin with $b_2 = \frac{a}{2}[\bar{1}01]$ or $\frac{a}{2}[0\bar{1}1]$. These two 60° dislocation arrays contribute the same total misfit edge components as an array of 90° dislocations with $b_{90} = \frac{a}{2}[\bar{1}\bar{1}0]$, as shown in the Fig 2(b). The period of dislocations in the observed two 60° arrays in Fig. 2(b) measured along the [110] direction is 5.6 nm, which corresponds to values reported on planar growth of GaSb on GaAs (001) with 90^0 Lomer dislocations [23, 24, 27].

Fig. 2(c) shows a fast Fourier transform (FFT) power spectrum of a TEM image with larger portion of the interface region including both faces of the fin. The FFT image shows perfect epitaxy, distinct lateral periodicities from GaAs and GaSb crystal lattices, and allows for evaluation of lattice spacings. The two lattices have the mismatch of $\delta = (a_{GaSb} - a_{GaAs})/a_{GaSb} = 7.3\%$, if $a_{GaSb} = 6.0959$ Å and if $a_{GaAs} = 5.6533$ Å are used, although in this structure thin GaAs can be under residual strain. Splitting of the FFT reflections (Fig. 2c) allows for relatively accurate measurements of the difference of the crystal periodicities of two materials: $\delta_{220} = 6.85\ (\pm\ 0.1)$ % and $\delta_{002} = 7.35\ (\pm\ 0.15)$ % indicating measurable residual strain and tetragonal distortion of the GaSb lattice. Assuming simple biaxial stress model (which might be not exactly correct due to in-plane anisotropy of the fin structure) the ratio of normal to lateral strains is $\varepsilon_{002}/\varepsilon_{220} = -2C_{12}/C_{11} = -0.9$. Therefore, the residual biaxial compressive stress in GaSb can be estimated as 0.25 ($\pm$ 0.1) %, if GaAs lattice is assumed not distorted. Another proof of the residual strain can be found in the inset of Fig. 2(c) showing the enlarged reflection splitting; GaSb spot is also split corresponding to two domains on the two sides of the fin with 1.5° tilt of crystal lattice. This lattice plane bending contributes to the relaxation of the residual stress as shown in Fig. 2(b).
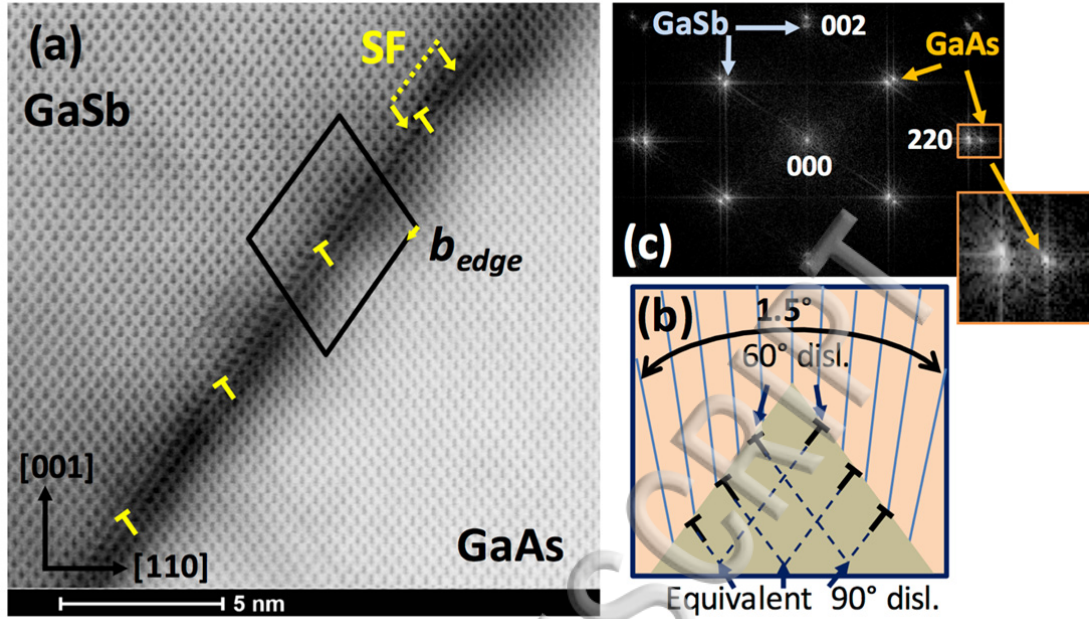
Figure 2: (a)_High resolution bright-field STEM image of the GaSb / GaAs interface showing periodic array of 60^0 dislocations along the $(\bar{1}\bar{1}1)$ interface imaged edge-on. The terminated (111) planes are indicated by "T"s. Burgers circuit is plotted by dark line; the closure gap corresponding to the edge component of the dislocation Burgers vector $b_{edge} = \frac{a}{4}[\bar{1}\bar{1}2]$, is shown by arrow. Two dissociated partials terminating stacking fault (SF) are indicated by arrows. (b) Schematics of two 60^0 dislocation arrays formed on the faces of a triangular-shaped fin. (c) FFT power spectrum of the micrograph.

In this specific case however, IMF formation might be further complicated by easy splitting of 60° dislocations into partials terminating stacking faults in between [29]. The {111} interface facets are most favorable for this splitting since it is not accompanied by the increase of strain energy as with the (001) planar interface. A close-up observation of the atomic dumbbell structure in Fig. 2(a) reveals the presence of twin (or stacking fault – SF) planes affecting two neighboring bilayers across the interface. Dark areas are located at the edges of the (13x1) GaSb cells around the dislocations and often coincide with the region at the interface where the SF are terminated and the atomic stacking shifts from the zinc-blend ABCABC sequence to ABCBCABC typical for intrinsic SF. The SF edges look gradual and involve 4-5 dumbbell rows, leading to a distortion of the zinc-blend structure where local stress builds up. Interfacial twinning normally involves only one bilayer at the time, but occasionally both interfacial bilayers are twinned, giving an ABCBABC stacking

corresponding to extrinsic SF. The width of SFs is likely limited by interaction of the partials in the misfit dislocation array.

Another typical feature related to the growth on {111} facets is nucleation of other type of planar defects, microtwins (MTs). Figure 3(a) reports one of these examples, where a 5 monolayer thick MT nucleates at the GaAs facet and propagates through the GaSb fin. The MTs nucleate easily as a result of their relatively low formation energy of about 10 mV/atom [31, 32], which can be normally overcome at the typical GaSb growth temperature. These accidental nucleation [33] results in propagation of the MTs through the growing film, but they are limited in the lateral direction by the domains nucleated in a correct stacking orientation; upon coalescence of the domains the MT platelets get terminated by the partial dislocation arrays as shown in Fig. 3(b). The growth-related MTs do not add to the strain relaxation (other than small contribution from relatively distant partials); no lattice misfit is needed for their nucleation as in the GaP/Si system [33]. These defects can be easily trapped at the trench oxide sidewalls through a careful design of the trench aspect ratio. Extensive TEM investigations on various trenches did not reveal any threading dislocations in the GaSb bulk.
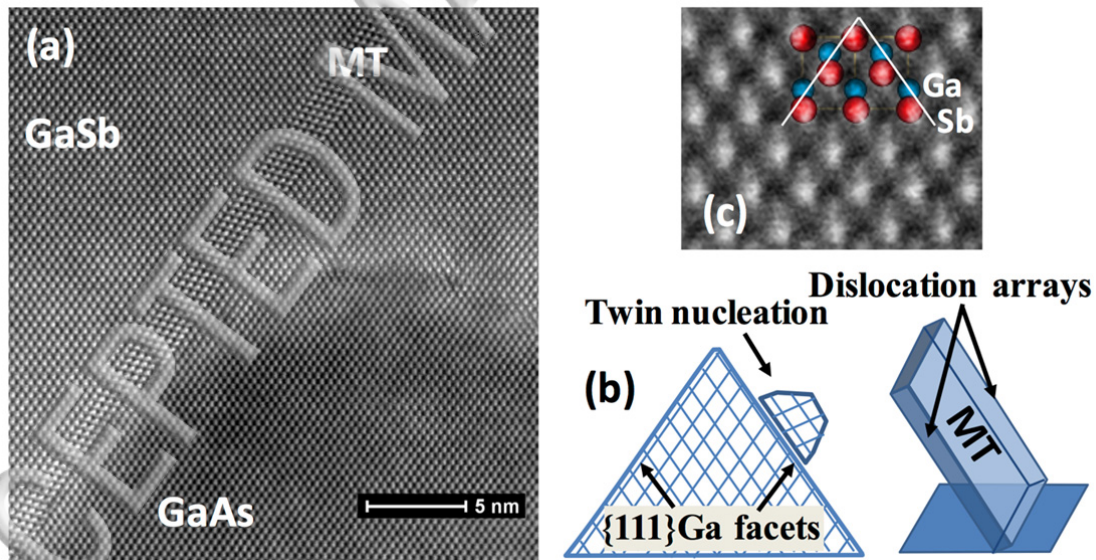

Figure 3: (a)_High resolution High-Angle Annular Dark-Field (HAADF) STEM image of the GaSb / GaAs interface showing 5 monolayers thick microtwin (MT) nucleated at the {111} Ga facets. (b) Schemeatics of a MT nucleation. (c) Magnified image of a portion of GaSb layer in (a) showing crystal polarity.

It should be also noted that our surface preparation and GaAs-on-Si nucleation techniques resulted in the growth of a specific polarity of the III-V materials. Fig 3(c) illustrates the polarity of the Ga-Sb dumbbells, where Sb atomic column with higher atomic number appears brighter than Ga atomic column under High resolution High-Angle Annular Dark-Field HAADF STEM imaging conditions. For this polarity, the GaAs fin facets are terminated by Ga and GaSb nucleation occurs on {111} Ga surfaces.

In order to demonstrate the potential of this approach in allowing the co-integration of different III-V materials on the same GaAs on Si template platform, we also attempted to deposit InAs layers. This material, together with GaSb, is considered to be a good candidate for replacing Si in the next generation CMOS technology [5]. The heteroepitaxy of InAs on GaAs (001) has been extensively studied, as the nucleation of InAs Quantum Dot (QD) structures allows the fabrication of lasers in the telecommunication wavelength range with improved performance and lower cost [34]. QDs form as a consequence of the stress generated by the lattice mismatch between the heteroepitaxial layer and the substrate, leading to 3D islanding. The InAs/GaAs system follows the Stranski–Krastanov growth mode, where the 2D growth of a highly strained layer changes in a 3D growth mode after about 2 MLs of InAs. One strategy to inhibit 3D islanding involves the use of a low temperature nucleation layer to promote the formation of a high density of small nucleation islands, whose slow coalescence generates a smooth and closed layer, in a quasi 2D growth mode [21]. Another way of avoiding 3D growth is through the heteroepitaxy of InAs on GaAs (111) surface where, in contrast with the (001) surface, the growth mode remains 2D for all InAs coverages [35, 36]. Therefore, the advantage of using {111} faceted GaAs as the growth template for InAs is that 3D islanding is suppressed, preventing the formation of defects due to coalescence of the 3D islands. This allowed us to keep the InAs growth temperature at 600 °C after the deposition of the GaAs buffer, and simply switch the group III precursor from TMGa to TMIn without interrupting the AsH$_3$ supply.
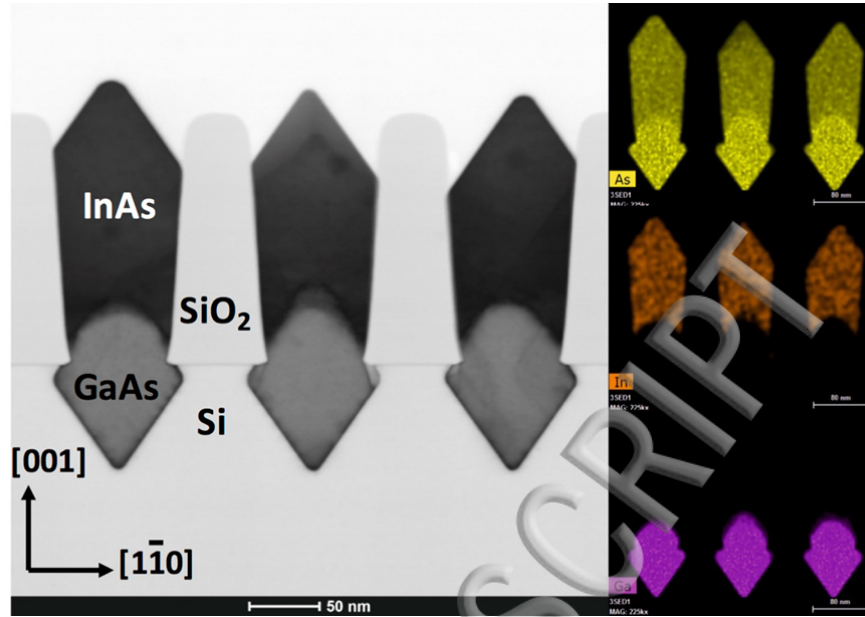
Figure 4: (a) Bright Field (BF) STEM image of the cross section of InAs on GaAs on Si fins along [1$\bar{1}$0], together with the Energy Dispersive X-Ray Spectroscopy STEM-EDS map of the Arsenic, the Indium and the Gallium Kα peaks.

Figure 4 shows the Bright Field (BF) STEM image of the cross section of InAs on GaAs on Si fins along [1$\bar{1}$0], together with the Energy Dispersive X-Ray Spectroscopy STEM-EDS maps of the Arsenic, the Indium and the Gallium Kα peaks. In order to increase the aspect ratio of the InAs fins, and allow a more efficient defect trapping than in the previous GaSb case, we reduced the GaAs growth time to target a thickness of 120 nm. As a consequence, GaAs {111} facets don't develop completely and a more rounded GaAs top is produced, which affects both GaAs and InAs morphology uniformity. In the specific case of the three InAs fins of Figure 4, the shape symmetry changes from one to another, suggesting the presence of {111} planar defects that influence the growth rate of the ($\bar{1}$11) and (1$\bar{1}$1) facets respectively. The height of InAs fins is ~ 150 nm, and they show well developed facets as a consequence of the higher growth temperature compared to GaSb. Figure 5 reports a high magnification bright-field STEM image of the InAs / GaAs interface, showing a sequence of ($\bar{1}\bar{1}$1) stacking faults (SFs) that propagate along the InAs fin but, given the high aspect ratio, annihilate against the oxide sidewalls. SFs originate in close proximity to the rounded GaAs top, suggesting the existence of several InAs merging fronts, likely associated with the high Miller index GaAs crystal planes that produce the rounding, where the growth rate and the

11

growth mode can be different from the 2D mode observed for the {111} planes. We believe that the morphology of InAs fins could be significantly improved by carefully controlling the formation of {111} GaAs facets. As demonstrated in the GaSb case, a GaAs height close to 150 nm seems to be a good compromise for this trench layout, as it guarantees well developed {111} facets and an aspect ratio high enough, for the half empty trench, to efficiently trap defects in the 6.1 Å family heteroepitaxial layer. Increasing the overall trench aspect from the actual 3 to a safer 4 would provide more flexibility in designing the III-V layer stack.
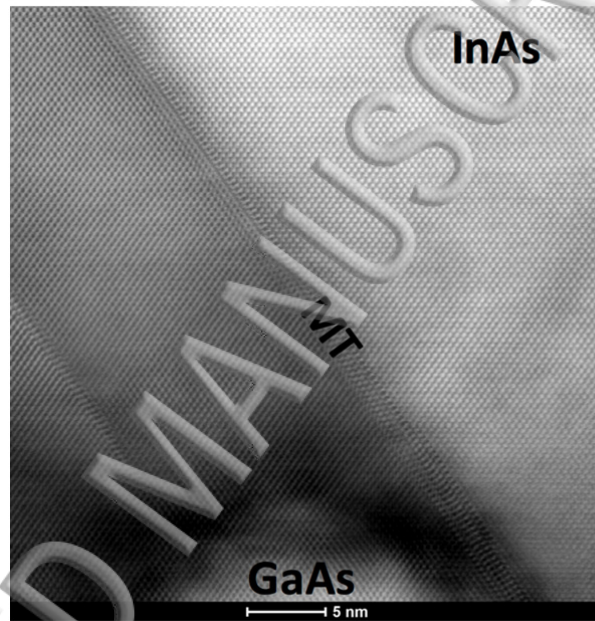
Figure 5: High resolution Bright Field (BF) STEM image of the InAs/GaAs interface showing stacking faults (SFs) and microtwins (MTs) originating in close proximity to the rounded GaAs top.

IV. CONCLUSIONS

In this study we demonstrate and elegant approach to integrate two important compound semiconductors belonging to the 6.1 Å family, namely InAs and GaSb, on 300 mm on-axis Si (001) wafers, using a common platform consisting of a thin, ~ 150 nm, GaAs buffer layer. The topmost part of the 6.1 Å family heteroepitaxial layers does not contain anti-phase

domains (APDs) or threading dislocations (TDs). APDs are avoided through a careful design of the GaAs / Si interface, as explained in detail in [21]. TDs in GaSb are controlled through the formation of an interfacial misfit (IMF) dislocation array along the GaSb / GaAs $[\bar{1}11]$ and $[1\bar{1}1]$ interfaces. Nonetheless, a few {111} microtwins originate at the interface but annihilate at the trenches' oxide sidewalls. Defects on InAs are controlled through the promotion of a 2-dimensional growth, which spontaneously occurs on GaAs {111} planes. However, the presence of high Miller index planes on the rounded GaAs fin top contribute to the formation of a secondary InAs growth front which likely produces planar defects when merging with the main growth front. Stacking faults are again trapped at the oxide sidewalls.

The deposition was done by MOCVD on large CMOS compatible on-axis Si (001) substrates, using a thin layer stack to manage thermal mismatch. Both achievements represent an important step forward towards the Very Large Scale Integration (VLSI) of high density III-V nano-scale photonic and electronic components with silicon circuits. Moreover, the flexibility of this approach can pave the way for the co-integration of p- and n-channel fin field-effect transistor (FinFET) based on high mobility 6.1 Å family compound semiconductors.
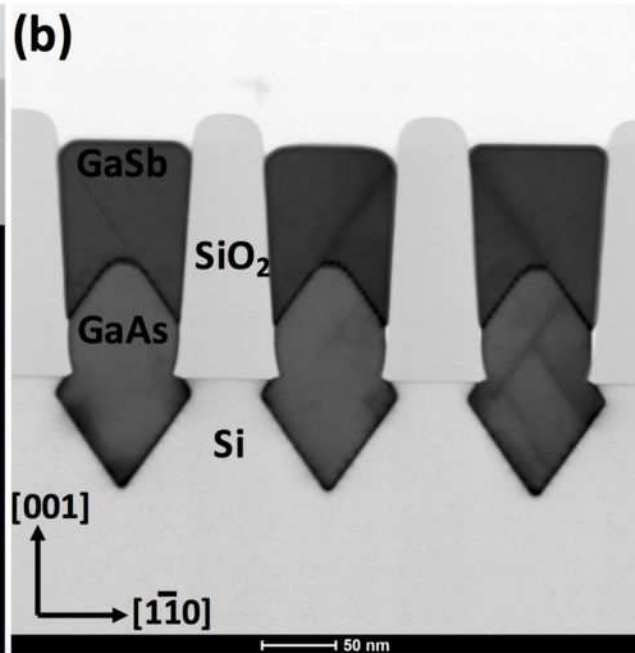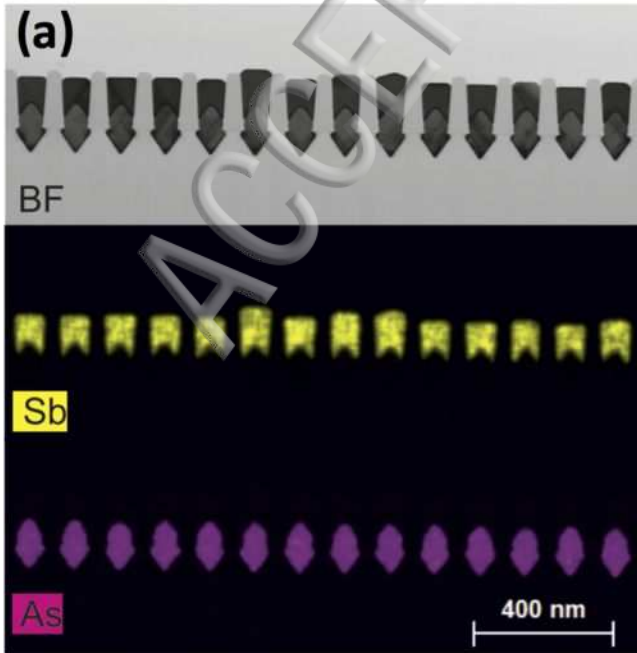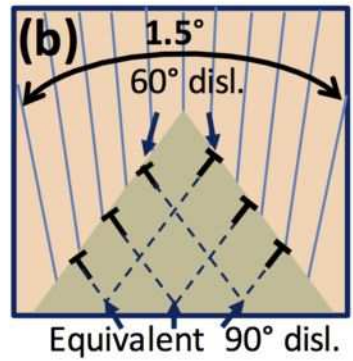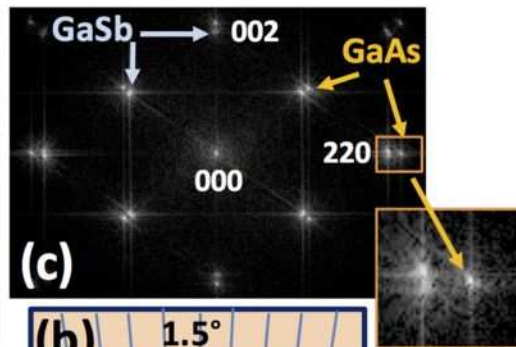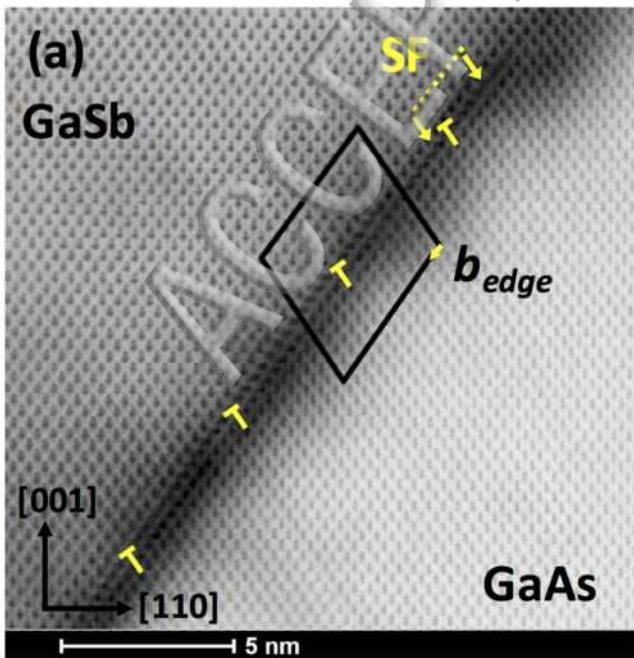
REFERENCES

[1] H. Kroemer, Physica E 20, 196 (2004), doi:10.1016/j.physe.2003.08.003

[2] L. F. Luo, R. Beresford and W. I. Wang, Appl. Phys. Lett. 55, 2023 (1989); http://dx.doi.org/10.1063/1.102151

[3] B.-M. Nguyen, S. Bogdanov, S. Abdollahi Pour and M. Razeghi, Appl. Phys. Lett. 95, 183502 (2009); http://dx.doi.org/10.1063/1.3258489

[4] G. Zhou, Y. Lu, R. Li, Q. Zhang, W. Hwang, Q. Liu, T. Vasen, H. Zhu, J. Kuo, S. Koswatta, T. Kosel, M. Wistey, P. Fay, A. Seabaugh, and H. Xing, Electron Devices Meeting (IEDM), p. 32.6.1 (2012) doi:10.1109/iedm.2012.6479154

[5] J. A. del Alamo, Nature, vol. 479, no. 7373, p. 317 (2011) doi:10.1038/nature10677

[6] M. Heyns et al. Electron Devices Meeting (IEDM), p.13.1.1 (2011), doi: 10.1109/iedm.2011.6131543

[7] W. Lu, J. K. Kim , J. F. Klem , S. D. Hawkins , J. A. del Alamo International Electron Devices Meeting (IEDM) p. 31.6.1 (2015), doi:10.1109/iedm.2015.7409810
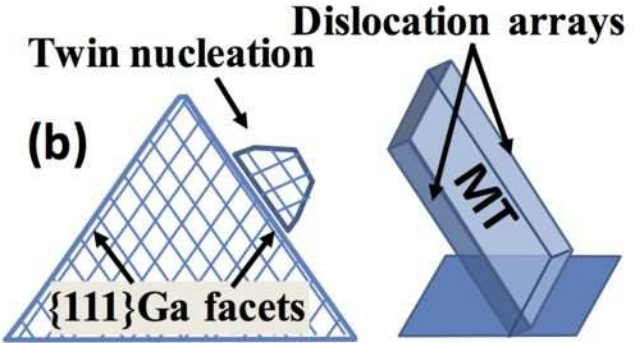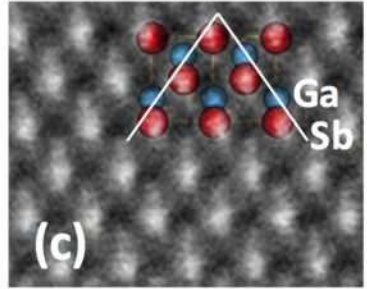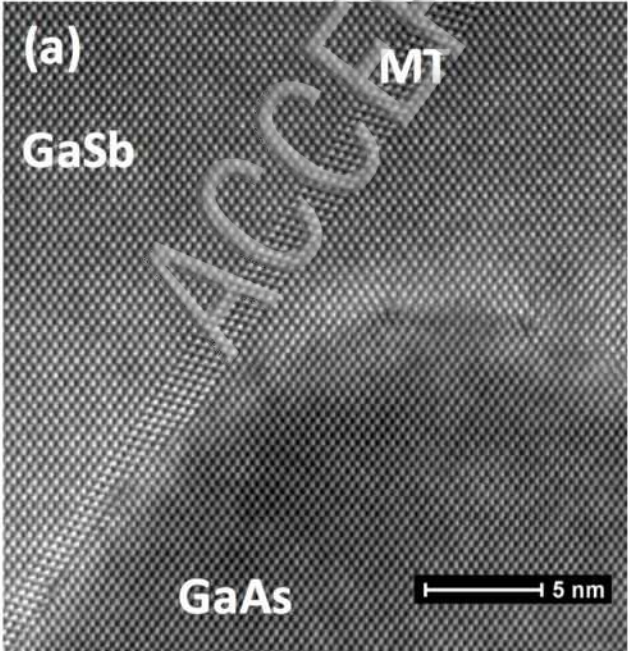
[8] T.-W. Kim, D.-H. Koh, C.-S. Shin, W.-K. Park, T. Orzali, C. Hobbs, W.P. Maszara, D.-W. Kim, Electron Device Letters, IEEE Volume: 36, Issue: 3, p.223, (2015) doi: 10.1109/led.2015.2393554

[9] H. Mohseni, E. Michel, Jan Sandoen, M. Razeghi, W. Mitchel and G. Brown , Appl. Phys. Lett. 71, 1403 (1997); doi: http://dx.doi.org/10.1063/1.119906

[10] D. L. Smith and C. Mailhiot J. Appl. Phys. 62, 2545 (1987), doi: http://dx.doi.org/10.1063/1.339468

[11] A. Gassenq, N. Hattasan, L. Cerutti, J. B. Rodriguez, E. Tournié, G. Roelkens, and G. Roelkens, Opt. Express 20(11), 11665, (2012), doi: 10.1364/OE.20.011665

[12] Y. C. Lin, H. Yamaguchi, E. Y. Chang, Y. C. Hsieh, M. Ueki, Y. Hirayama and C. Y. Chang, Appl. Phys. Lett. 90, 023509 (2007); doi: http://dx.doi.org/10.1063/1.2431567

[13] K.-M. Ko, J.-H. Se, D.-E. Kim, S.-T. Lee, Y.-K. Noh, M.-D. Kim and J.-E. Oh, Nanotechnology 20 225201, (2009) doi:10.1088/0957-4484/20/22/225201

[14] K. Akahane, N. Yamamoto, S. Gozu, N. Ohtani, J. Crystal Growth 264, 21, (2004) doi:10.1016/j.jcrysgro.2003.12.041

[15] G. Balakrishnan, S. Huang, L.R. Dawson, Y.-C. Xin, P. Conlin, D.L. Huffaker, Appl. Phys. Lett. 86, 034105, (2005) DOI: 10.1063/1.1850611

[16] H. Toyota, T. Sasaki, Y. Jinbo, N. Uchitomi, Journal of Crystal Growth 310, 78, (2008) doi:10.1016/j.jcrysgro.2007.10.008

[17] Rodriguez J.B., Cerutti L., Grech P., Tournié E.; Appl. Phys. Lett. 94, 061124 (2009); http://dx.doi.org/10.1063/1.3082098

[18] Cerutti L, Rodriguez J.B., Tournié E.; IEEE Photonics Technology Letters 22, p.553, (2010) DOI:10.1109/LPT.2010.2042591

[19] K. Volz, A. Beyer, W. Witte, J. Ohlmann, I. Németh, B. Kunert, and W. Stolz, J. Cryst. Growth 315(1), 37 (2011); http://dx.doi.org/10.1016/j.jcrysgro.2010.10.036

[20] L. Desplanque, S. El Kazzi, C. Coinon, S. Ziegler, B. Kunert, A. Beyer, K. Volz, W. Stolz, Y. Wang, P. Ruterana and X. Wallart, Appl. Phys. Lett. 101, 142111 (2012); http://dx.doi.org/10.1063/1.4758292

[21] T. Orzali, A. Vert, B. O'Brien, J. L. Herman, S. Vivekanand, R. J. W. Hill, Z. Karim and S. S. Papa Rao; J. Appl. Phys. 118, 105307 (2015); doi: http://dx.doi.org/10.1063/1.4930594

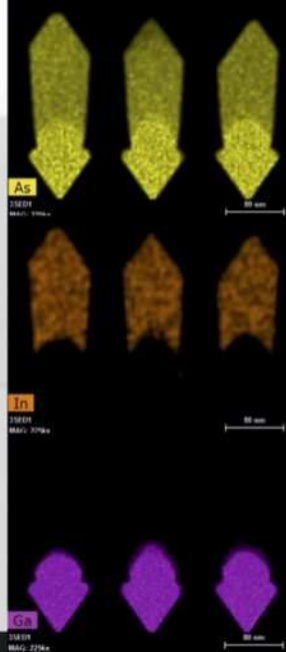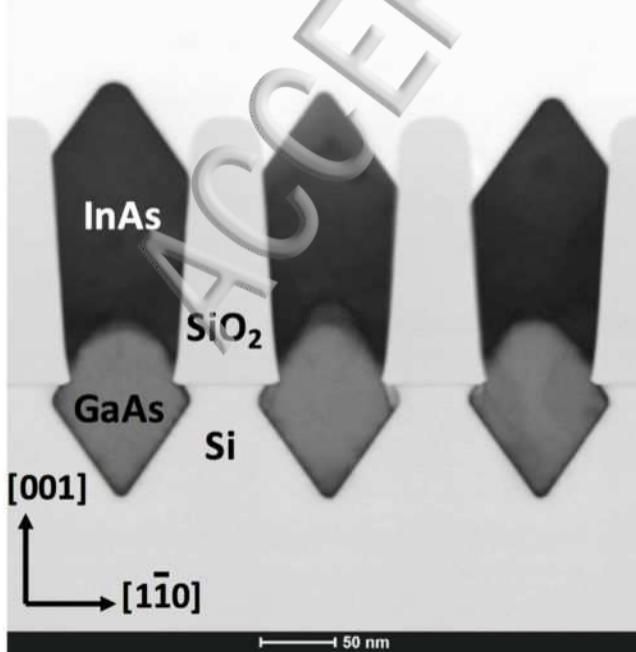[22] M. Lee, D. J. Nicholas, K. E. Singer, B. Hamilton, J. Appl. Phys. 59 (8) 2895 (1986); doi: 10.1063/1.336948

14

[23] S. H. Huang, G. Balakrishnan, A. Khoshakhlagh, A. Jallipalli, L. R. Dawson, and D. L. Huffaker, Applied Physics Letters 88, 131911 (2006); doi: 10.1063/1.2172742

[24] Yi Wang, P. Ruterana, S. Kret, J. Chen, S. El Kazzi, L. Desplanque, and X. Wallart, Applied Physics Letters 100, 262110 (2012)

[25] S. Madisetti, V. Tokranov, A. Greene, S. Novak, M. Yakimov, S. Oktyabrsky, S. Bentley and A.P. Jacob; MRS Proc., 1635, T02.03 (2014), DOI: http://dx.doi.org/10.1557/opl.2014.219

[26] S. K. Madisetti, V. Tokranov, A. Greene, M. Yakimov, M. Hirayama, S. Oktyabrsky, S. Bentley, A. P. Jacob, J. Vac. Sci. Technol. B **32**(5), 051206 (2014); doi: http://dx.doi.org/10.1116/1.4892797

[27] W. Zhou, X. Li, S. Xia, J. Yang, W. Tang and K.M. Lau, J. Mater. Sci. Technol., 28(2), 132 (2012)

[28] W. Zhou, W. Tang, and K. M. Lau, Applied Physics Letters 99, 221917 (2011), doi:10.1063/1.3663571

[29] J. Narayan and S. Oktyabrsky, J. Appl. Phys., 92, pp. 7122-7, (2002) doi: http://dx.doi.org/10.1063/1.1521789

[30] A. Jallipalli, G. Balakrishnan, S.H. Huang, A. Khoshakhlagh, L.R. Dawson, D.L. Huffaker, Journal of Crystal Growth 303, 449, (2007), doi:10.1016/j.jcrysgro.2006.12.032

[31] C.Y. Yeh, Z.W. Lu, S. Froyen, A. Zunger. Physical Review B. 45(20), 12130, (1992) DOI:http://dx.doi.org/10.1103/PhysRevB.45.12130

[32] Glas, F. J. Appl. Phys. 104, 093520 (2008) http://dx.doi.org/10.1063/1.3009338

[33] F. Ernst, P. Pirouz. J. Appl. Phys. 64, 4526 (1988); http://dx.doi.org/10.1063/1.341280

[34] S. Chen, W. Li, J. Wu, Q. Jiang, M. Tang, S. Shutts, S. N. Elliott, A. Sobiesierski, A. J. Seeds, I. Ross, P. M. Smowton and H. Liu, Nature Photonics (2016) doi: 10.1038/nphoton.2016.21

[35] H. Yamaguchi, M.R. Fahy, and B.A. Joyce, Appl. Phys. Lett. 69, 776 (1996); http://dx.doi.org/10.1063/1.117888.

[36] S. E. Hooper, D. I. Westwood, D. A. Woolf, S. S. Heghoyan and R. H. Williams, Semicond. SC J Technol. 8, 1069, (1993)

(a) BF, Sb, As — scale bar 400 nm.

(b) GaSb, SiO₂, GaAs, Si. Directions [001], [1̄10]. Scale bar 50 nm.

(a) GaSb, GaAs, SF, b_{edge}, [001], [110], 5 nm

(b) 1.5°, 60° disl., Equivalent 90° disl.

(c) GaSb, 002, GaAs, 220, 000

(a) GaSb, MT, GaAs — scale bar 5 nm

(b) Twin nucleation, Dislocation arrays, {111}Ga facets, MT

(c) Ga, Sb

InAs

SiO₂

GaAs

Si

[001]

[1̄10]

As

In

Ga

50 nm

InAs

MT

GaAs

5 nm